Journal of Materials Science: Materials in Electronics (2019) 30:6669–6679
https://doi.org/10.1007/s10854-019-00976-z

Metal (II) complexes with derived from 3-hydroxy-2-(3-nitrophenyl)-4*H*-chromen-4-one; synthesis and photocatalytic activity

Sakthivadivel Rajendran[1] · Xavier Arulantham[1] · Pandi Pitchai[2,3] · Siva Sundarajan[4]

Received: 12 December 2018 / Accepted: 19 February 2019 / Published online: 27 February 2019

Abstract
The synthesized novel flavonol was studied by ^{1}H NMR spectroscopy, ^{13}C NMR spectroscopy, FTIR, GC–mass spectrometry. And moreover, the metal complexes (M = Fe, Ni, Cu) with TiO_2 nanocomposites are synthesized and studied by UV–Vis–NIR spectroscopy, GC–mass spectrometry, UV–Vis–DRS, XRD profile, SEM and TEM techniques. The performance of photocatalytic degradation of malachite green (MG) under visible light irradiation by Metal (M = Fe, Ni, Cu,) complex of 3-hydroxy-2-(3-nitrophenyl)-4*H*-chromen-4-one of nanocomposite was studied. In photocatalytic degradation of MG, the detail investigations are made by the effect of catalyst concentration; initial MG concentration and addition of inorganic salts. The MG photo degradation result of different ML–TiO_2 is as follows Cu(II) > Fe(II) > Ni(II). Interestingly, the CuL–TiO_2 has better photocatalytic efficiency of 97% as compared to the other ML–TiO_2 in visible light at 80 min. The adsorption malachite green on ML–TiO_2 was found to boost by the Langmuir and Freundlich approach.

1 Introduction

Most of the industrial waste dyes are harmful to the surrounding environment. Among these organic pollutants, MG has been considerable attention due the stable chemical behavior of the environment. Removal of organic/inorganic pollutant from the ecosystem is a great challenge to the researchers. In the past few decades, the researcher identified TiO_2 has a substantial role in the removal of the later said pollutants. On the other hand, TiO_2 as the photocatalyst have (i) low sensitivity in the range of visible region (ii) high rate of recombination of photogenerated electron–hole pair. The above identified problems of TiO_2 are removed in recent research by organic/inorganic composites. Because of the absorption is shifted towards the higher frequency, which means that the greater the photon energy gives more energy to the photogenerated electron–hole pair. Recently numerous research articles are published for the removal of environmental hazards by the process of photocatalytic activity, such as *N*-benzyl-ocarboxymethyl Chitosan magnetic nanoparticles [1] Halloysite nanotubes [2] Amino functioned graphemes [3] Fibrous sodium titanate [4] poly GMA/DVB [5]. Among them, surface modified TiO_2 by metal complexes have better photocatalytic activity. The efficient performance of coordination metal complexes are takes place as functional materials for the enhanced adsorption and photodegradation [6–8]. Because of the metal complexes are acting as high energy photon sensitizer for efficient the photocatalytic activity of semiconductors. Metal complexes (ML) materials are an effect of combination of ML and TiO_2 (ML–TiO_2 or ML/TiO_2), it has attractable structures, large surface areas, microporous sizes and adsorbate–ML interaction sites [9]. Moreover, pore volume utilizing catenation and creation of open metal sites and incorporation of different functional groups in metal complexes at octahedral environment. Because the correlation between metal complex structures and potential properties [10–12]. In general the functional properties of metal complexes are depends on their pores. In this research paper, to examine for novel photocatalyst with suitable conditions a complete photodegradation of the organic pollutants can be achieved and the general mechanisms are also investigated.

✉ Pandi Pitchai
pandipmc11@gmail.com

[1] PG and Research Department of Chemistry, The Madura College, Madurai 625 011, India

[2] PG and Research Department of Physics, The Madura College, Madurai 625 011, India

[3] Department of Solar Energy, School of Energy Sciences, Madurai Kamaraj University, Madurai 625021, India

[4] PG and Research Department of Chemistry, Thiagarajar College, Madurai 625 009, India

2 Materials and methods

2.1 Synthesis of ligands (3-hydroxy-2-(3-nitropheny l)-4*H*-chromen-4-one)

4-Nitrobenzaldehyde and 1-(2-hydroxyphenyl) ethanone in 1:1 molar ratio were mixed and refluxed over a water bath for complete the reaction. The resulting chalcone separated out upon cooling, and then further add 30% H_2O_2 and NaOH. The resulting Flavonol was filtered, washed with ethyl acetate, and dried.

3-Hydroxy-2-(4-nitrophenyl)-4*H*-chromen-4-one, 60c mp, 206–209° C (aq.ethanol); yield: 90% UVλ_{max} (MeOH): 372 nm, IR (Fig. 2a) (KBr, cm^{-1}): 3080.32 (OH-3), 1757.14 (C=O), C–N (str) 1601.78, 1541.12, 1517.98. ^{1}H NMR (Fig. 2b) (500 MH_Z, $CDCl_3$): δ 6.57–7.72 (m, 8H, Ar–H), 11.23 (s, 1H, OH-3). ^{13}C NMR (Fig. 2b) (125 MHz, $CDCl_3$): δ 114.91, 121.78, 122.55, 123.22, 124.97, 136.02, 138.43, 144.03, 155.83, 171.17, (CO). *Anal.Calcd for* $C_{15}H_9NO_5$: C 63.61; H 3.20, found: C 63.65%; H 3.22%. The mass of the molecular ion (M+) at m/z 283.04 ((M–OH)+), base peak at m/z 221 ((M–OH)+), suggesting the presence of OH group. The position of the OH group at C (3) is evident from retro-Diels–Alder fragment ion at m/z 121 (A, +H) and 105 (B_2^+).

2.2 Synthesis of metal complex ($C_{15}H_9$ M NO_5): (M = Cu, Fe, Ni)

The complex was prepared in a moderate yield from the reaction of $MCl_2{\cdot}2H_2O$ with the prepared ligand in 1:2M ratio. The ligand (0.61 g, 2 mM) dissolved in methanol was added slowly to a methanolic solution of $MCl_2{\cdot}2H_2O$ (0.24 g, 1 mM) with continuous stirring which was followed by a change in the color of solution to brown. After for 24 h at room temperature, a brown precipitate obtained was separated out. This precipitate was then washed with hexane and dried in vacuo. The scheme of synthesis is shown in Fig. 1.

Yield 69% m.p. 279° C. Anal. (%) Calc. For ($C_{15}H_9$ Cu NO_5): C, 62.02; H, 3.63; Cu, 9.94; N, 4.38; O, 20.03. Molar conductance, (1×10^{-3} M, methanol): 210 Ω^{-1} cm^2 mol^{-1} (1:2 electrolytes). From the Fig. 2a, selected IR data on KBr pellet (γ/m cm^{-1}); 1705.70 (C=O); 1266.18 (NO_2); 749.14 (Cu–O); UVλ_{max} (MeOH): 350 nm. Figure 3a reveals that the ESI–MS (m/z) 346.68 $[C_{15}H_9NO_5Cu]^+$ (m/z) 629.90[$(C_{30}H_{16}N_2O_{10})_2$Cu].

Yield 65% m.p. 254° C. Anal. (%) Calc. For ($C_{15}H_9$ Fe NO_5): C, 62.77; H, 3.66; Fe, 8.84; N, 4.44; O, 20.27. Molar conductance, (1×10^{-3} M, methanol): 180 Ω^{-1} cm^2 mol^{-1} (1:2 electrolytes). Moreover Fig. 2a selected IR data on KBr pellet (γ/m cm^{-1}); 1718.12 (C=O); 1278.96 (NO_2); 761.92 (Fe–O); UVλ_{max} (MeOH): 347 nm. Figure 3b illustrates that the ESI–MS (m/z) 347 $[C_{15}H_9NO_5Fe]^+$ (m/z) 631[$(C_{30}H_{16}N_2O_{10})_2$ Fe].

Yield 68% m.p. 265° C. Anal. (%) Calc. For ($C_{15}H_9$ Ni NO_5): C, 62.49; H, 3.66; Ni, 9.25; N, 4.42; O, 20.27. Molar conductance, (1×10^{-3} M, methanol): 150 Ω^{-1} cm^2 mol^{-1} (1:2 electrolytes). As shown in Fig. 2a, selected IR data on KBr pellet (γ/m cm^{-1}); 1744.16 (C=O); 1227.17 (NO_2); 723.59 (Ni–O); UVλ_{max} (MeOH): 328 nm. Figure 3c shows that the ESI–MS (m/z) 341 $[C_{15}H_9NO_5Ni]^+$ (m/z) 624[$(C_{30}H_{16}N_2O_{10})_2$Ni]$^+$.

2.3 Synthesis of metal complex modified TiO_2 (ML–TiO_2) nanoparticles

ML–TiO_2 was synthesized from dispersing 0.1 g of Metal complex and 3 g of TiO_2 in 50 ml of chloroform. This mixture was taken in a round bottom flask equipped with a reflux condenser. The whole mixture was refluxed at 70 °C for 3 h. After that the mixture was cooled, filtered and repeatedly washed with chloroform to remove the unreacted metal complex. The resulting solid was dried in an oven at 100 °C for 1 h.

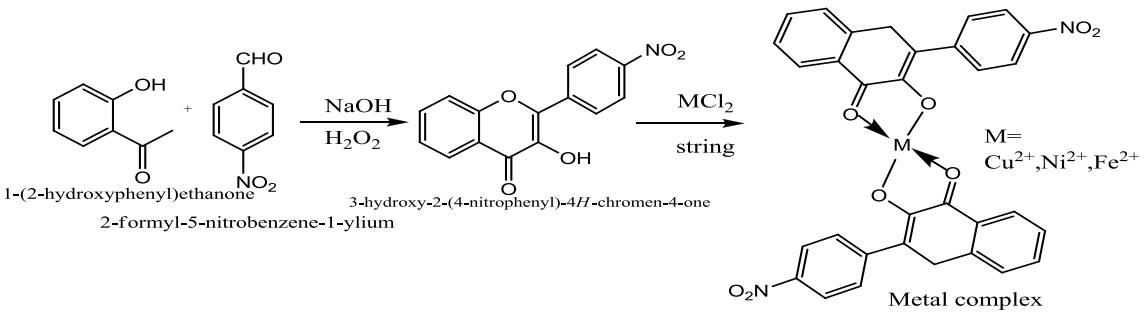

Fig. 1 The scheme of synthesis of 3-hydroxy-2-(3-nitrophenyl)-4*H*-chromen-4-one and Cu(II) complex, Fe(II) complex and Ni(II) complex 3-hydroxy-2-(3-nitrophenyl)-4*H*-chromen-4-one

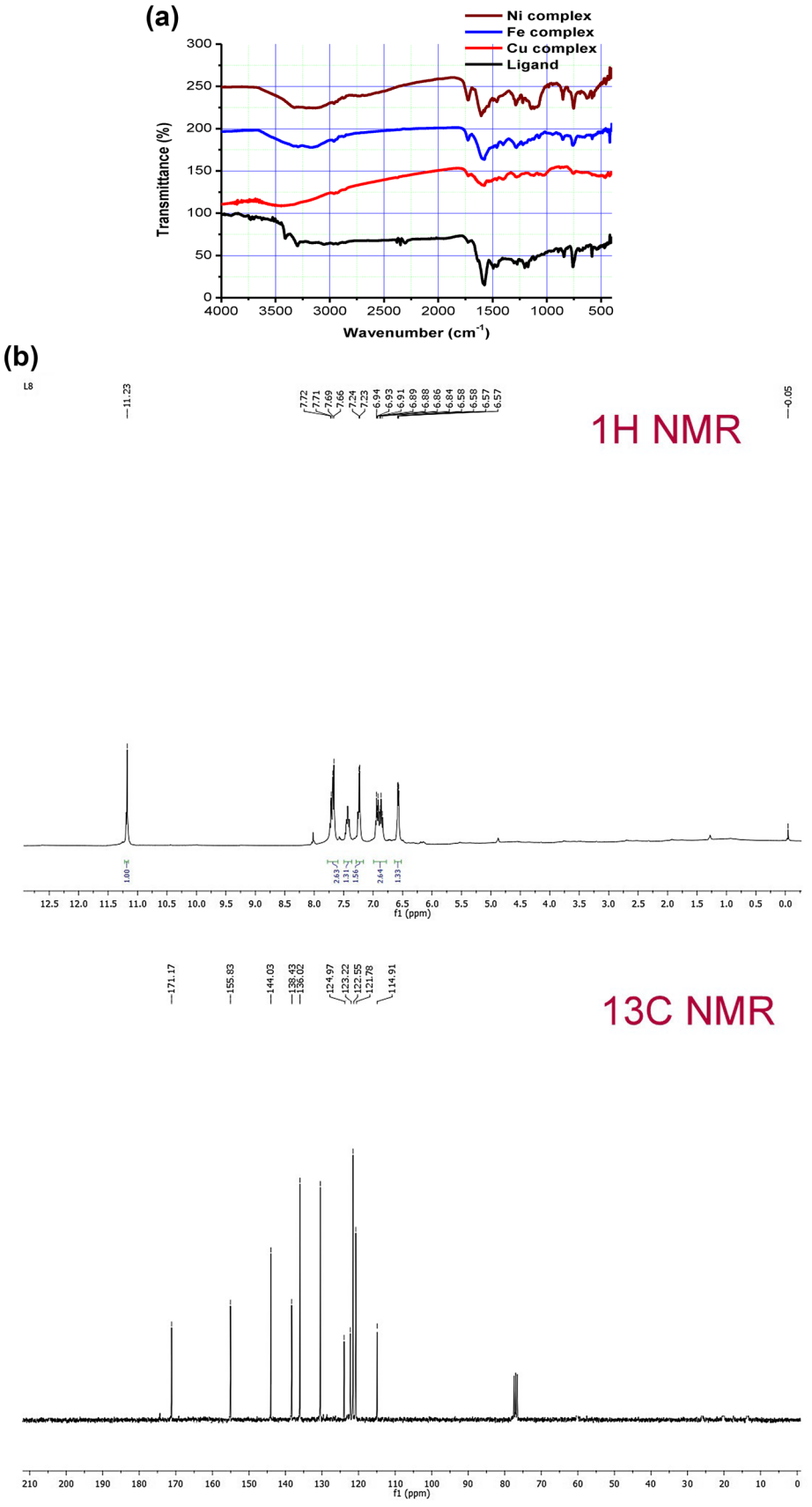

Fig. 2 **a** FTIR spectrum of Ligand and their Metal complexes. **b** ^{1}H NMR spectrum and C^{13} NMR spectrum of 3-hydroxy-2-(3-nitrophenyl)-4*H*-chromen-4-one

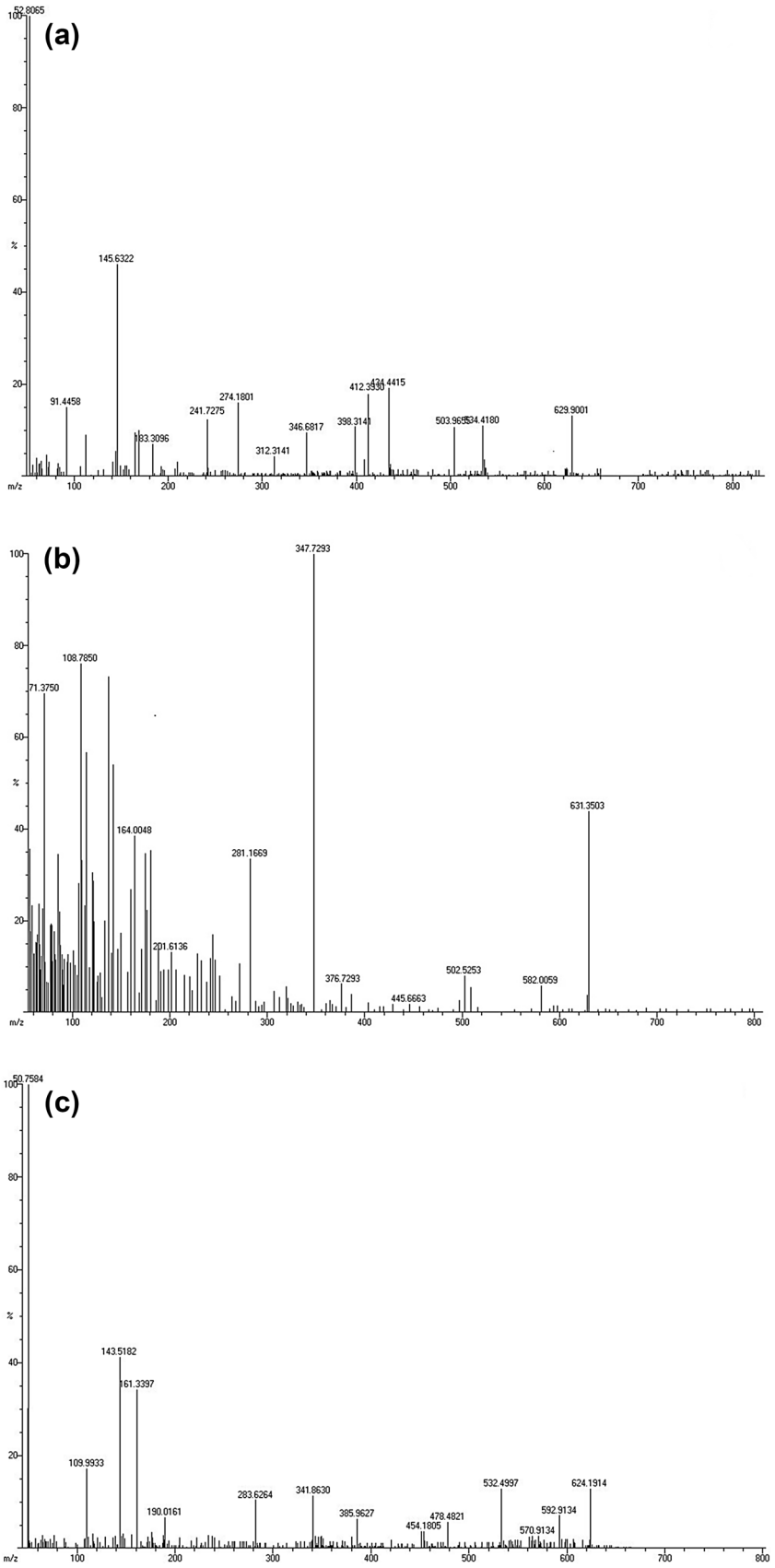

Fig. 3 Mass spectrum of **a** Cu(II) complex, **b** Fe(II) complex and **c** Ni(II) complex 3-hydroxy-2-(3-nitrophenyl)-4*H*-chromen-4-one

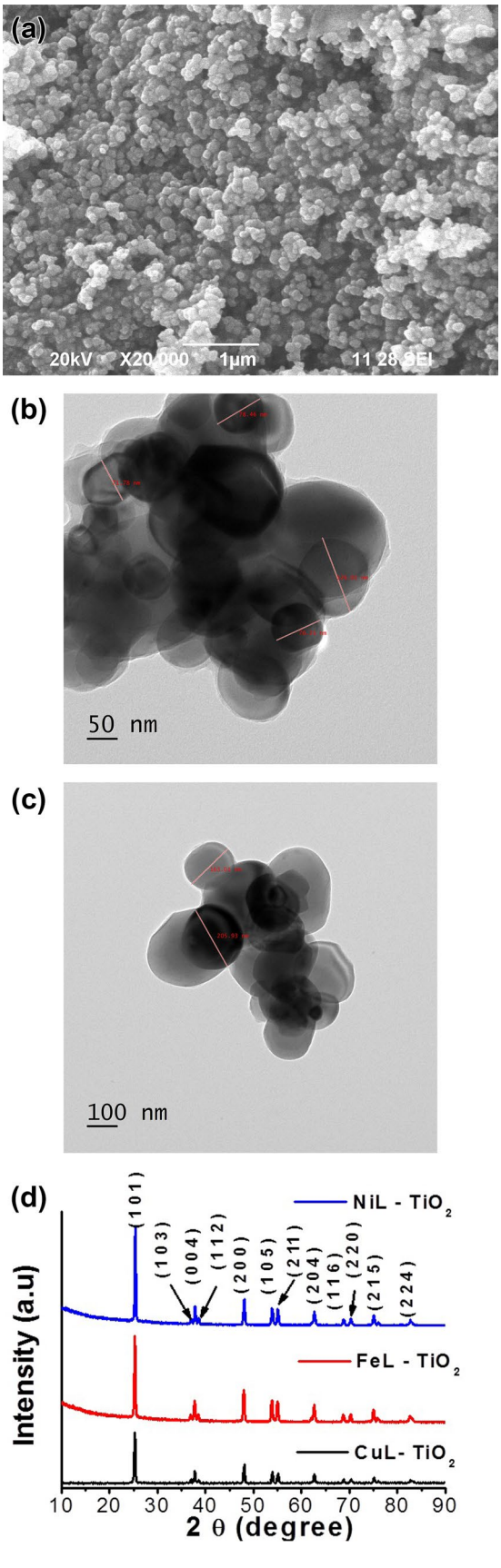

Fig. 4 **a** SEM image of Cu L–TiO_2 nanoparticles. **b** TEM image of Fe L–TiO_2 nanoparticles. **c** Ni L–TiO_2 nanoparticles size distribution. **d** XRD pattern of synthesized ML–TiO_2

3 Result and discussion

ML (Cu, Fe and Ni)—TiO_2 nanoparticles are studied form the SEM and TEM. Figure 4a as it can be seen in the spherical like morphology with uniform size of CuL–TiO_2 sample show particles with great aggregation. Figure 4b, c, the typical TEM images of the Fe and Ni metal complex TiO_2 nanoparticles indicates that the TiO_2 nanoparticles are uniform in size with agglomerates of 5–10 crystallites and highly crystalline TiO_2 aggregates composed of nanoparticles with particle size of 71–126 nm for Fe metal complex TiO_2 and 100–206 nm for Ni metal complex TiO_2. The XRD pattern of the ML (Cu, Fe, and Ni)-TiO_2 (Fig. 4d) illustrates the sharp peaks are observed at diffraction angles 2θ value for ML–TiO_2 (JCPDS card # 21-1272). The average crystallite size of CuL-TiO_2, FeL-TiO_2 and NiL-TiO_2 is determined as 34 nm, 31 nm and 46 nm using the Scherer's formula respectively.

$$D = \frac{K\lambda}{B\cos\theta}$$

B is the Full Width at Half Maximum in radians. K is a constant. λ is the wavelength, D is the crystallite size and θ is the Bragg angle [13].

UV–Vis DRS, free TiO_2 has a strong absorption in the region of 397 nm which was greatly improved after being sensitized by NiL–TiO_2, FeL–TiO_2 and CuL–TiO_2 leading to the red shift of absorption towards the visible region. The absorption efficiency of the photocatalysts is analyzed by Tauc approach. The optical band gaps are highly suitable for receiving visible light. The energy band gap of the Metal complex (C_{15} H_9 M NO_5)-TiO_2 are determined by extrapolation of the linear portion of the curves of $(\alpha hv)^2$ vs hv as shown in Fig. 5 [14]. The intra ligand bands are slightly shifted to longer wavelength upon complexation with metal ions. The $n \rightarrow \pi^*$ (forbidden transition) takes place in 3-hydroxy-2-(3-nitrophenyl)-4*H*-chromen-4-one is due to unsymmetrical nuclear vibrations, but in Metal complexes (Fig. 1.) $\pi \rightarrow \pi^*$ (allowed transition) is occurred by symmetrical nuclear vibrations. The shift of the π –π^* bands to for the longer wavelength region the metal complexes are due to the C=O and N=O bond being weakened and its act as a flurophores the enhanced conjugation system on complexation. Tauc plot of Fig. 5 gives band gap of 2.39 eV, 2.26 eV, 2.15 eV, for ML–TiO_2 (M = Cu^{2+}, Ni^{2+} and Fe^{2+}) and it showing small variation, may be due to the rigid phenyl cores in three compounds are inert and also supports the fact that the two O atoms of the carbonyl moiety are the nodal points in the arrangement of the valance band (VB)

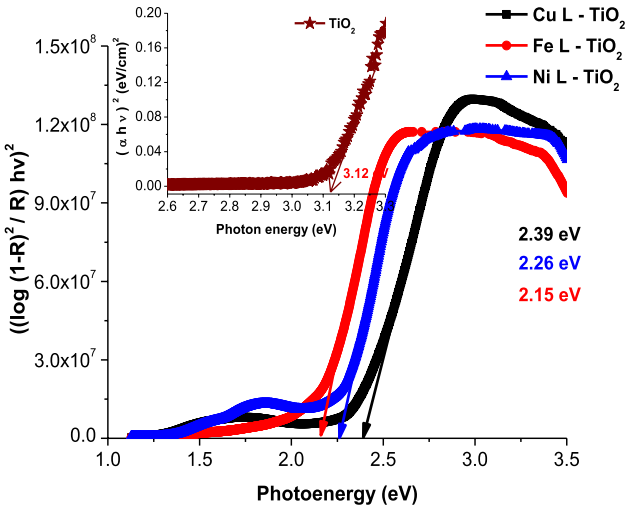

Fig. 5 Tauc extrapolation graph of ML–TiO_2 (M = Cu^{2+}, Ni^{2+} and Fe^{2+})

and conduction band (CB) of the orbitals [15]. The decreasing band gap level from TiO_2 to ML–TiO_2, more number of electrons able to transfer from valance band to conduction band compare to the naked TiO_2 (3.12 eV). Synthesized ML–TiO_2 has significantly absorption intensity the visible region compared to the free TiO_2 [Ti^{4+} has no unpaired electron in distorted octahedron structure (Fig. 6a)], which is due to the ligand to metal charge transfer (LMCT) from ML to Ti (Ti^{3+} has only one d-electron in octahedron structure (Fig. 6b)) and it is result shows octahedral coordination structure [13]. Finally, band gap decreased from 3.12 to 2.39 eV, 2.26 eV and 2.15 eV and it shows that photosensitizer nature of the ML was adsorbed on the surface of TiO_2.

4 Photocatalytic mechanism of MG

ML–TiO_2 gives rise to bright colours associated with transition metal complexes in case of ML–TiO_2, Ti^{3+} complex ion (Ti^{3+} has only one d-electron) the light of the wavelength in the visible region of the spectrum as shown in Fig. 6b, c. In ML–TiO_2 when light is absorbed by a complex ion, an electron in one of the lower energy to higher energy. The energy corresponding to the frequency of the absorbed light is equal to energy in octahedral environment. Metal complexes is performed as a photosensitizer and transfer the electrons to ML–TiO_2 heterojunction, narrows the band gap of TiO_2, hinders the electron–hole pairs recombination, extends the work in visible light, and increase the photocatalytic activity of catalyst. The photocatalyst mainly involve the formation and reaction of ·OH radicals.

4.1 Adsorption studies through batch approach

Figure 7 is designated clearly that the % of adsorption of MG increased with increasing the amount of adsorbents from 0.005 to 0.020 g L^{-1} due to the subsistence of adsorbents site for the adsorption of MG from polluted aqueous solution. Consequently there is not major increase in the % of adsorption after 0.020 g/L since moves persistently from 0.020 to 0.040 g/L due to no availability of adsorption sites in the all adsorbents.

Batch approach used for studying the Adsorption works by shaking 0.020 g of the adsorbents like CuL–TiO_2, FeL–TiO_2, NiL–TiO_2 and TiO_2 in 40 mL solution of MG with 180 ppm concentration for 50 min in the rotator water bath shaker at 250 rpm stirring rate. Then the effect of initial metal-ion concentration and contact time were also determined for the MG adsorption onto various adsorbents. MG concentration in the supernatants after the adsorption onto the different adsorbents was calculated with UV–visible spectrophotometer. The equilibrium adsorption capacity of the all adsorbents was found with this equation:

$$q_e = \left(C_o - C_e\right) \times V/M \quad (1)$$

Where q_e is the equilibrium adsorption capacity (mg g^{-1}), Co and C_e is the initial and final MG concentration (mg L^{-1}) at equilibrium, V is the volume of solution (L) and M is the weight (g) of adsorbent [16].

4.2 Adsorption isotherm analysis

Figure 8 indicated that the C_O raises from 30 to 180 mg L^{-1} due to the initial concentration creates essential driving force by the development of concentration gradient between the bulk solution and surface of the four adsorbents [17]. No significant enhance in the adsorption capacity of the four adsorbents beyond 180 mg/L due to the saturation of surface active sites over it. The mechanism between MG and four adsorbents can be identified by the various adsorption isotherm models as Freundlich and Langmuir isotherm models. The values were found from the Figs. 8, 9a, b, 10a, b, 11a, b, 12a, b and are tabulated in Tables 1 and 2:

$$\text{Freundlich isotherm}: \log q_e = \log K_F + (1/n)\log C_e \quad (2)$$

$$\text{Langmuir isotherm: } (Ce/q_e) = \left(1/Q_o b\right) + \left(Ce/Q_o\right) \quad (3)$$

Where K_F (mg g^{-1}) is the Freundlich constant and 'n' the Freundlich exponent. Where q_e (mg g^{-1}) is the adsorbed amount of MG at equilibrium, C_e (mg L^{-1}) is the equilibrium concentration of MG, Q_o (mg g^{-1}) and b (L mg^{-1}) are Langmuir constants related to adsorption capacity and energy of

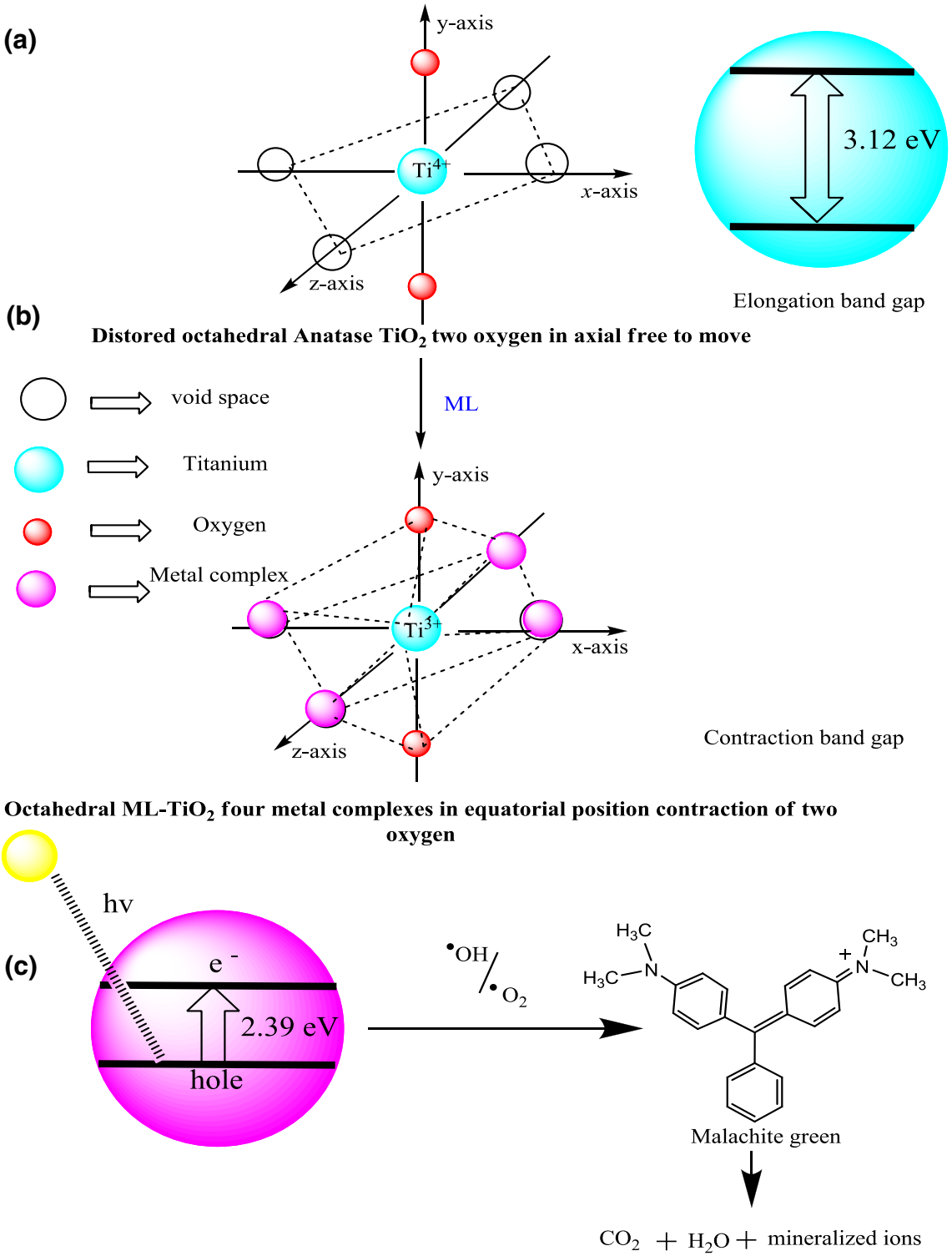

Fig. 6 Schematic representation of **a** Distorted octahedral of anatase phase of TiO_2. **b** Octahedral ML–TiO_2 (M = Cu^{2+}) and **c** photocatalytic pathway of ML–TiO_2

adsorption. Then the Langmuir isotherm noteworthy value as separation factor (R_L) can be calculated with the Eq. 4.

$$R_L = 1/(1 + bQ_o) \quad (4)$$

The R_L value supposed the nature with feasibility of adsorption process is stated in Table 1. The calculated high R^2 value proved that the adsorption of MG on four

adsorbents can be fitted well with Langmuir isotherm as evaluated to the Freundlich isotherm. The R_L value (Table 3) ranges from 0 to 1 proved that the adsorption process is favorable for the four adsorbents [18]. Moreover, CuL–TiO_2 exhibited a superior adsorption activity as compared to the other three adsorbents. The value of the n greater than 1 suggested that the concerned environments for adsorption. The adsorption capacities of the four adsorbents and former adsorbents for the removal of MG from aqueous solution or wastewater are stated in Table 4 [1–5].

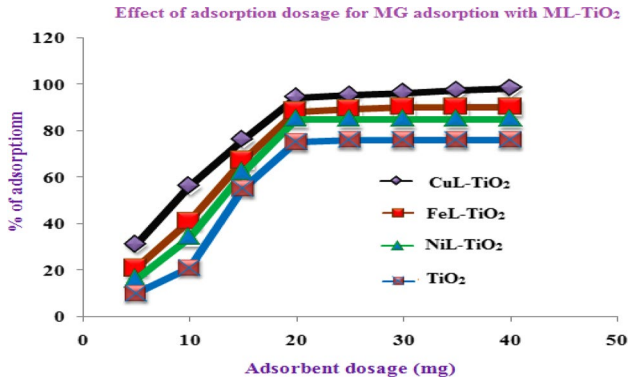

Fig. 7 Effect of adsorbent dosage

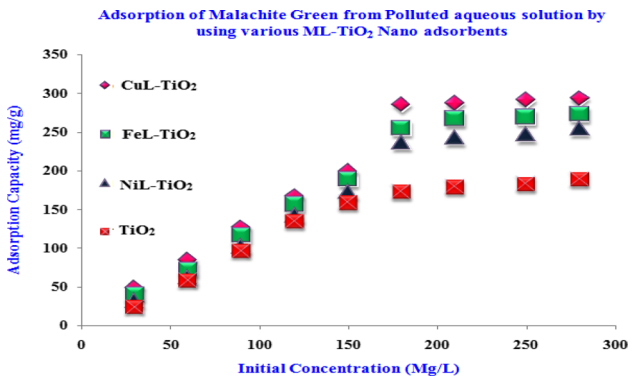

Fig. 8 Effect of concentration on the removal of MG from aqueous solution

4.3 Adsorption kinetics study

Figure 13 clearly suggested that the adsorption process was quick at the beginning of reaction and over in 50 min. As a result, extended successive point for the MG adsorption on four adsorbents was stopped in 80 min. Thus the stability time was 50 min for this adsorption. Further, no considerable change was found due to the happening of more active sites on four adsorbents at the start of reaction and more active sites were not presented on four adsorbents after 50 min. The pseudo-first-order and pseudo-second-order kinetic representations were exploited to inform like adsorption.

$$\mathrm{Log}\left(q_e - q_t\right) = \log q_e - \left[k_1/2.303\right] t \quad (5)$$

$$t/q_t = 1/k_2 q_e^{\,2} + t/q_e \quad (6)$$

Where k_1 is the pseudo-first-order rate constant (min^{-1}), q_e (mg g^{-1}) is the adsorption capacity at equilibrium, q_t (mg g^{-1}) is the adsorbed amount of MG after time t (min), k_2 is the pseudo- second-order rate constant (g mg^{-1} min^{-1}). The all values were determined from Fig. 14a, b as well as tabulated in Table 5. The calculated R^2 values of the four adsorbents for pseudo second-order kinetic model is upper than the pseudo-first order kinetic model and then the experimental q_e values of the four adsorbents are extremely closer to the determined q_e value for pseudo-second-order kinetic model as compared to Pseudo-first-order kinetic model. Hence the adsorption processes of the four adsorbents were followed Pseudo second order kinetic model [19]. Then the adsorbent CuL–TiO_2 displayed better adsorption results while compared to the other adsorbents.

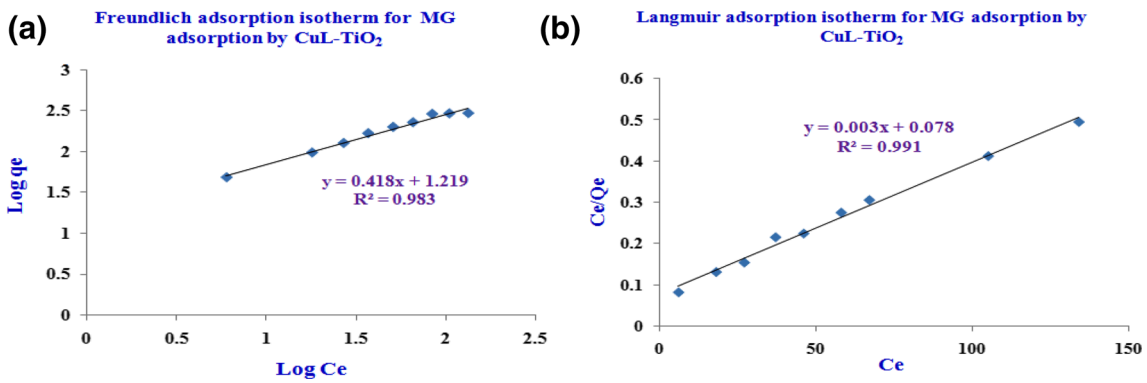

Fig. 9 Freundlich (**a**) and Langmuir plots (**b**) for MG removal by CuL–TiO_2

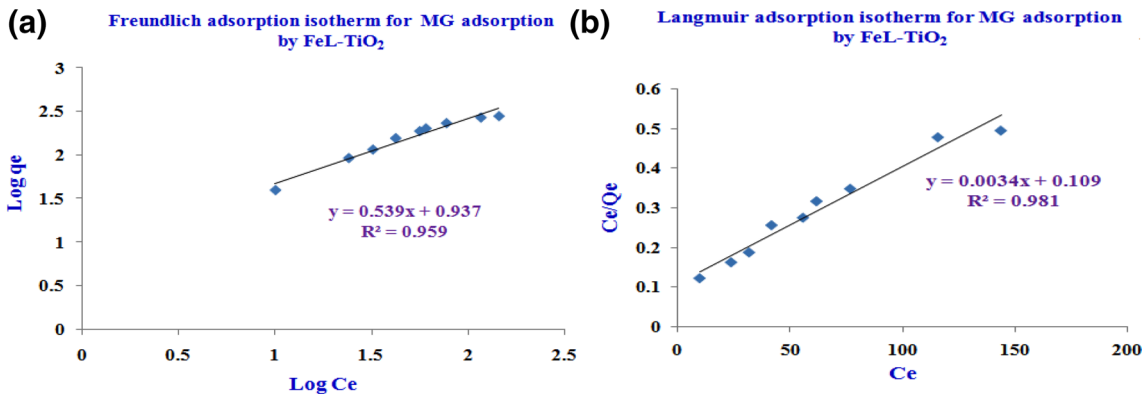

Fig. 10 Freundlich (**a**) and Langmuir plots (**b**) for MG removal by FeL–TiO_2

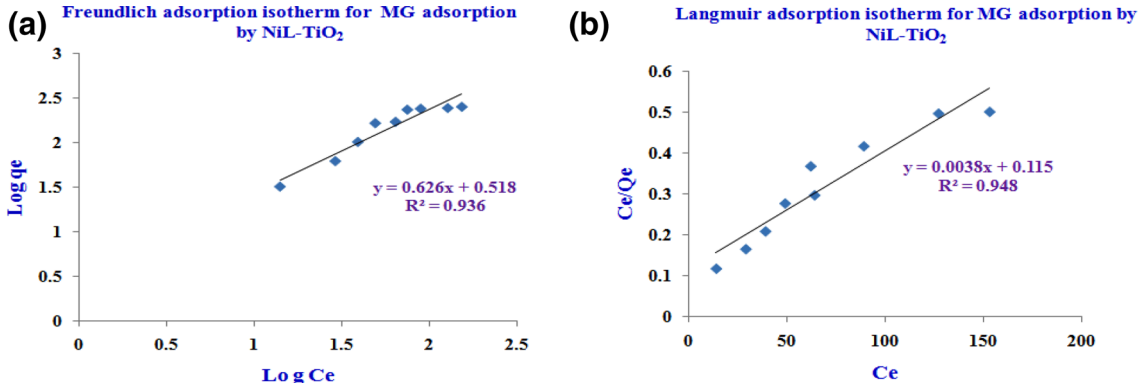

Fig. 11 Freundlich (**a**) and Langmuir plots (**b**) for MG removal by NiL–TiO_2

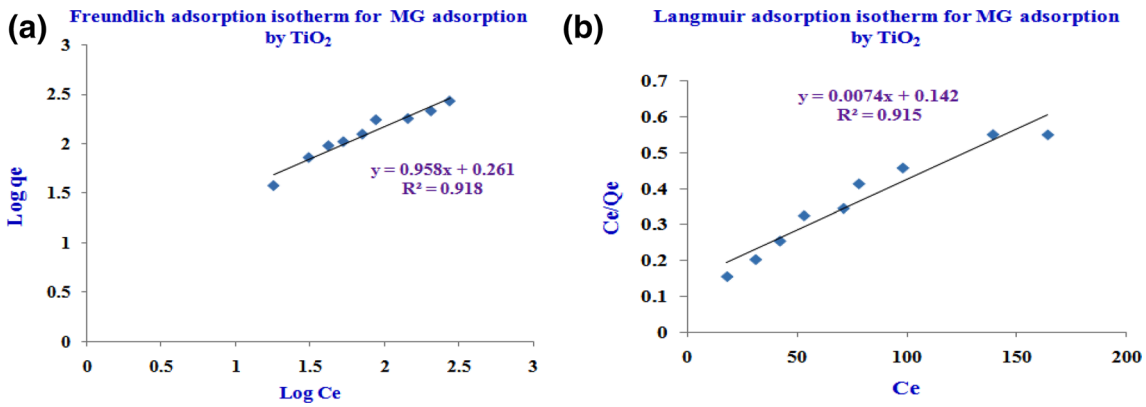

Fig. 12 Freundlich (**a**) and Langmuir plots (**b**) for MG removal by TiO_2

5 Conclusion

The successfully synthesized three metal complex materials, CuL–TiO_2, FeL–TiO_2 and NiL–TiO_2 under Sol–gel conditions by the reaction of transition metal chloride salts and flavonol of synthesized organic compound (L:3-hydroxy-2-(3-nitrophenyl)-4*H*-chromen-4-one). Through three complexes materials were characterized by UV–Vis

Table 1 Freundlich isotherm factors for MG removal onto the adsorbents

Freundlich isother factors	CuL–TiO_2	FeL–TiO_2	NiL–TiO_2	TiO_2
N	2.3923	1.8552	1.5974	1.038
K_F	16.5576	8.6496	3.2960	1.8238
R^2	0.983	0.959	0.936	0.918

Table 2 Langmuir isotherm factors for MG removal onto the adsorbents

Langmuir isother factors	CuL–TiO_2	FeL–TiO_2	NiL–TiO_2	TiO_2
Q_o	333.33	294	263.15	135.13
b	0.0384	0.0312	0.0330	0.0521
R_L	0.0723	0.0982	0.103	0.1243
R^2	0.991	0.981	0.948	0.915

Table 3 Nature of adsorption isotherm and the feasibility

R_L value	Adsorption process
$R_L > 1$	Unfavourable
$R_L = 1$	Linear
$0 < R_L < 1$	Favourable
$R_L = 0$	Irreversible

Table 4 Comparison of adsorption capacities of different adsorbents with ML–TiO_2

Adsorbent	MG	References
N-Benzyl-ocarboxymethylchitosan magnetic nanoparticles	144.79	[1]
Halloysite nanotubes	99.6	[2]
Amino functionalized graphenes	91.48	[3]
Fibrous sodium titanate	261.38	[4]
poly GMA/DVB	13.6	[5]
CuL–TiO_2	**333.33**	Present work
FeL–TiO_2	**294**	Present work
NiL–TiO_2	**263.15**	Present work
TiO_2	**135.13**	Present work

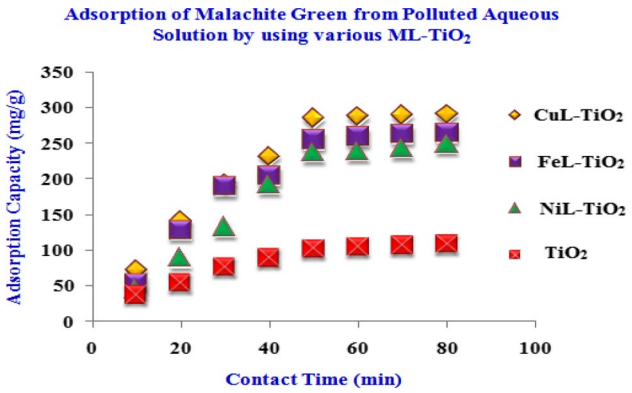

Fig. 13 Effect of contact time on the removal of MG from aqueous solution

spectra, IR spectra, ^{1}H NMR spectroscopy, ^{13}C NMR spectroscopy, GC-MASS spectrometry, XRD analysis and HRTEM. The UV–Vis spectra showed that the three complexes were octahedral structures with band gap ranges 2.15–2.39 eV.

In addition we investigated the photodegradation ability of the three complexes for malachite green dye under Visible light. The result showed that three complexes had different degradation ability to MG solution. Further we found that the degradation process was in accordance with pseudo-second-order kinetic model and the correlation constant is as high as 0.9–0.99, which indicates that the rate of adsorption is takes place on surface adsorption. The most significant is that the adsorption capacity of copper complexes (CuL–TiO_2) can reach 0.020 g when the MG concentration is 180 ppm and time 50 min. Therefore, these may have a potential effect on our degradation of MG in wastewater.

The electronic configuration of copper(II) ion has Jahn teller distortion, which make excellent candidates for carry stable and more electrons by changing the redox potential as compared to the other metals in the complexes. Copper(II) complex of 3-hydroxy-2-(3-nitrophenyl)-4*H*-chromen-4-one high frequency sensitive photocatalyst. CuL–TiO_2 platform exhibited a superior performance based on all respects especially on adsorption activities compared to other three adsorbents. Hence the built up CuL–TiO_2 can be applied efficiently for the elimination of high concentration MG from polluted aqueous solution and waste water in textile industries.

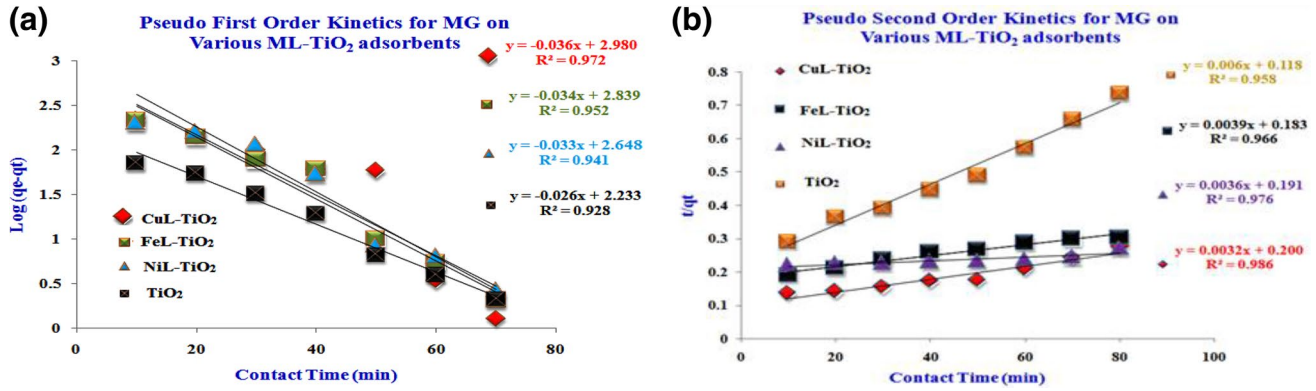

Fig. 14 **a** Pseudo I order, **b** Pseudo II order kinetics for MG removal by ML–TiO_2

Table 5 Pseudo first and second order kinetics for MG removal onto the adsorbents

Pseudo order of kinetics parameters	CuL–TiO_2		FeL–TiO_2		NiL–TiO_2		TiO_2	
	I	II	I	II	I	II	I	II
q_e	954.99	312.5	690.23	277.77	444.63	256.41	215.27	166.66
K_1	0.0829	5.12×10^{-5}	0.0783	6.78×10^{-5}	0.0759	8.31×10^{-5}	0.0460	3.05×10^{-4}
R^2	0.972	0.986	**0.952**	0.976	0.941	0.966	0.928	0.958

References

1. A. Debrassi, A.F. Correa, T. Baccarin, N. Nedelko, A. Slawska-Waniewska, K. Sobczak, P. Dłużewski, J.M. Greneche, C.A. Rodrigues, Chem. Eng. J. **183**, 284–293 (2012)
2. G. Kiani, M. Dostali, A. Rostami, A.R. Khataee, Adsorption studies on the removal of malachite green from aqueous solutions onto halloysite nanotubes. Appl. Clay Sci. **54**, 34–39 (2011)
3. X. Guo, Q. Wei, B. Du, Y. Zhang, X. Xin, L. Yan, H. Yu, Removal of basic dyes (malachite green) from aqueous medium by adsorption onto amino functionalized graphenes in batch mode, Desalin. Water Treat. **53**, 818–825 (2015)
4. J. Huang, M. Zhao, H. Chen, L. Dong, X. Guo, X. Liu, Preparation of fibrous sodium titanate and its adsorption property toward neutral red, methylene blue, malachite green and crystal violet, Optoelectron. Adv. Mater. **9**, 471–477 (2015)
5. D. Husaain, M. Najam-ul-Haq, A. Saeed, F. Jabeen, M. Athar, M.N. Ashiq, Synthesis of poly GMA/DVB and its application for the removal of malachite green from aqueous medium by adsorption process, Desalin. Water Treat. **53**, 2518–2528 (2015)
6. S.G. Chen, Z.Z. Shi, L. Qin, H.L. Jia, H.G. Zheng, Photodeegradation of some organic dyes over metal-organic frameworks with especially high efficiency for safranine T. Cryst. Growth Des. **17**, 67–72 (2017)
7. P.D.C. Dietzel, H. Kitagawa, Metal-organic frame work- heading towards applications. Eur. J. Inorg. Chem. **27**, 4267–4270 (2016)
8. A.V.I. Desai, B. Manna, A. Karmakar, A. Sahu, S.K. Ghoush, A water-stable cationic metal-organic framework as a dual adsorbent of oxoanion pollutants. Angew. Chem. Int. Ed. **55**, 7811–7815 (2016)
9. H.L. Jiang, Xu, Porous metal-organic frame works as platforms for functional applications. Q. Chem. Commun. **47**, 3351–3370 (2011)
10. C.J. Doonan, D.J. Tranchemontagne, T.G. Glover, J.R. Hunt, O. Yaghi, M.Nat. Exceptional ammonia uptake by a covalent organic frame work. Chem. **2**, 235–238 (2010)
11. H.X. Deng, C.J. Doonan, H. Furukawa, R.B. Ferreira, J. Towne, C.B. Knobler, B. Wang, Yaghi, Multiple fuctioanl groups of varying ratios in metal-organic frame works. O. M. Science **327**, 846–850 (2010)
12. J.R. Li, R.J. Kuppler, H.C. Zhou, Selective gas adsorption and separation in metal- organic frame works. Chem. Soc. Rev. **38**, 1477–1504 (2009)
13. P. Pandi, C. Gopinathan, Synthesis and Characterization of TiO_2–NiO and TiO_2–WO_3 nanocomposites. J. Elect. Mater. **28**, 7, 5222–5234 (2017)
14. Y. Dong Jianga, D. Xua, Y. Wua, Suna, Visible-light responsive dye-modified TiO_2 photocatalyst. J. Solid State Chem. **181**, 593–602 (2008)
15. F. Farukh Arjmand, M. Sayeed. Muddassir, Synthesis of new chiral heterocyclic Schiff base modulated Cu(II)/Zn(II) complexes: their comparative binding studies with CT-DNA, mononucleotides and cleavage activity. J. Photochem. Photobiol. B **103**, 166–179 (2011)
16. S.D. Khattri, M.K. Singh, Colour removal from dye wastewater using sugar cane dust as an adsorbent. Adsorpt. Sci. Technol. **17**, 269–282 (1999)
17. O. Hamdaoui, Batch study of liquid-phase adsorption of methylene blue using cedar sawdust and crushed brick. J. Hazard. Mater. **135**, 264–273 (2006)
18. S.S. Tahir, N. Rau, Removal of a cationic dye from aqueous solutions by adsorption on to bentonite clay. Chemosphere **63**, 1842–1848 (2006)
19. J. Zhang, Y. Li, C. Zhang, C. and Y. Jing, Adsorption of malachite green from aqueous Solution onto carbon prepared from Arundo donax root. J. Hazard. Mater. **150**, 774–782 (2008)